alloys

MDPI

Article

Assessing the Corrosive Effects of Unmelted Particles in Additively Manufactured Ti6Al4V: A Study in Simulated Body Fluid

Surinder Pal [1,*], Xavier Velay [1] and Waqas Saleem [2]

[1] Department of Mechanical and Manufacturing Engineering, Atlantic Technological University, F91 YW50 Sligo, Ireland; xavier.velay@atu.ie
[2] School of Mechanical Engineering, Technological University Dublin, D07 EWV4 Dublin, Ireland; waqas.saleem@tudublin.ie
* Correspondence: surinder92.pal@gmail.com

Abstract: This study investigates the corrosion behavior of Grade 23 Ti6Al4V alloys produced through laser powder bed fusion (L-PBF) when exposed to simulated body fluid at room temperature, focusing on the role of unmelted particles. This research aims to understand how these microstructural features, resulting from the additive manufacturing process, influence the corrosion resistance of the alloys. It was observed that unmelted particles serve as critical sites for initiating localized corrosion, including pitting, which significantly compromises the material's overall durability. Electrochemical testing and detailed surface analysis revealed that these particles, alongside other defects such as voids, exacerbate the susceptibility to corrosion in biomedical environments where high material reliability is paramount. Weight loss measurements conducted over exposure periods of 48 h, 96 h, and 144 h demonstrated a progressive increase in corrosion, correlating with the presence of unmelted particles. These findings underscore the importance of optimizing L-PBF processing parameters to minimize the formation of unmelted particles, thereby enhancing corrosion resistance and extending the operational lifespan of Ti6Al4V implants in biomedical applications.

Keywords: L-PBF; Ti6Al4V; corrosion; AM; pitting

Citation: Pal, S.; Velay, X.; Saleem, W. Assessing the Corrosive Effects of Unmelted Particles in Additively Manufactured Ti6Al4V: A Study in Simulated Body Fluid. *Alloys* **2024**, *3*, 257–268. https://doi.org/10.3390/alloys3040015

Academic Editor: Pavel Krakhmalev

Received: 31 July 2024
Revised: 23 September 2024
Accepted: 24 September 2024
Published: 9 October 2024

1. Introduction

The use of titanium alloys, particularly Ti Grade 23 (Ti6Al4V), in biomedical applications has gained prominence due to their favorable mechanical properties, including high strength-to-weight ratio, excellent biocompatibility, and superior corrosion resistance [1–3]. These properties make Ti6Al4V an ideal candidate for implants such as dental fixtures, joint replacements, and bone plates [4,5]. Recent advancements in manufacturing technologies, notably laser powder bed fusion (L-PBF), have further enhanced the applicability of Ti6Al4V alloys by enabling the creation of complex geometries and customized implant designs [6,7]. L-PBF is an additive manufacturing technique that utilizes a high-powered laser to selectively melt and fuse metal powder layers into a solid structure [8]. This method offers significant advantages over traditional subtractive manufacturing processes, including reduced material waste and the ability to produce highly precise structures [9,10]. Additionally, direct energy deposition (DED) [11] and cold spraying (CS) [12] are two further additive manufacturing techniques used for producing Ti6Al4V components. While DED is capable of producing parts with high deposition rates, it has the drawback of causing increased oxidation in the material. In contrast, cold spraying offers a solid-state deposition method but suffers from lower geometric accuracy when compared to L-PBF.

However, despite these advantages, the corrosion behavior of Ti6Al4V produced via L-PBF has raised concerns. Corrosion resistance is a critical factor in the longevity and performance of implants, as degradation of the material can lead to implant failure and

adverse biological reactions [13,14]. Qian et al. [15] studied the corrosion resistance of Ti6Al4V, which can be changed by the L-PBF process, as influenced by its microstructure. Similarly, Sola et al. [16] stated that the rapid cooling rates and complex thermal gradients inherent in L-PBF can lead to the formation of microstructural defects, such as voids, pores, and unmelted particles. These defects can act as initiation sites for localized corrosion, particularly in aggressive environments like simulated body fluid [17]. Previous studies have demonstrated that even minor defects can significantly impact the corrosion resistance of titanium alloys, leading to pitting and stress corrosion cracking [18–21].

Understanding the corrosion behavior of Ti6Al4V fabricated by L-PBF is crucial for optimizing manufacturing parameters to enhance the material's performance in biomedical applications. Recent research has highlighted the need for thorough investigations into how different L-PBF processing conditions affect corrosion resistance. For example, Zhao et al. [22] investigated how the alterations in laser power, scanning speed, and layer thickness can influence the formation of microstructural defects and, consequently, the material's susceptibility to corrosion. Additionally, Attar et al. [23] highlighted that microstructure, mechanical properties, wear resistance, and process parameters significantly influence the corrosion behavior of materials produced by L-PBF. Understanding the correlation between L-PBF settings and material characteristics is crucial for enhancing industrial applications. Surface defects in additive manufacturing, such as roughness, morphology inconsistencies, unmelted powder particles, the balling effect, and surface deformations, are well-documented challenges [24].

While there is substantial research on the electrochemical properties of L-PBF samples [25,26], there is limited focus on the impact of unmelted particles on the corrosion behavior of L-PBF Ti6Al4V in SBF under ambient conditions. This study explores how exposure to SBF affects the surface morphology and corrosion of L-PBF-fabricated Ti6Al4V. Given the importance of mechanical and corrosion properties for biomedical applications of 3D-printed Ti6Al4V, a thorough understanding of these characteristics is essential. This study employs scanning electron microscopy and electrochemical analysis for characterization. The primary objective is to assess the corrosion behavior of Grade 23 Ti6Al4V alloys produced via L-PBF, specifically focusing on the role of unmelted particles and microstructural defects in promoting localized corrosion. This research seeks to clarify the relationship between L-PBF processing parameters, microstructural attributes, and corrosion resistance by conducting electrochemical tests and surface analyses on samples exposed to SBF. The findings are expected to inform the optimization of L-PBF parameters, thereby reducing corrosion issues and enhancing the reliability of Ti6Al4V implants in clinical settings.

2. Materials and Methods

The chemical composition of the Ti6Al4V used, determined according to ASTM E29 Standards [27], is shown in Table 1. Three samples, each measuring 20 × 20 × 20 mm^3, were produced for this study. The Ti6Al4V was manufactured using powder particles with an average size of 20–60 µm, exhibiting a particle size distribution ranging from 26 µm (d10), 46 µm (d50), and 59 µm (d100) sourced from AP&C Powder Metallurgy in Boisbriand, Canada. The bulk density of the powder was 2.51 g/cm^3 (ASTM B212-21 [28]). These samples were prepared using the "EOS M 280 Metal Print, Waterford, Ireland" machine, equipped with a 200 W solid-state laser operating in an argon atmosphere [29]. Each sample was ground to a 120-grit finish before being exposed to a simulated body fluid (SBF) solution maintained at 37 °C. Surface roughness (Ra) of the Ti6Al4V samples was measured using a Surfcom Touch 50 surface profilometer prior to exposure to assess its potential influence on the material's corrosion behavior. The pH of the solution was adjusted to 7.30, aligning with the normal pH range of human body fluids, which is typically between 7.35 and 7.45 [30]. The L-PBF parameters used are detailed in Table 2. The L-PBF-fabricated Ti6Al4V samples were immersed in SBF for 48 h, 96 h, and 144 h.

Table 1. Chemical composition Ti6Al4V powder.

Item	Al	V	Fe	O	C	N	H	Y	Ti
wt. %	6.41	3.93	0.21	0.08	0.01	0.03	0.002	<0.40	Balance

Table 2. Used process parameters to fabricate L-PBF samples.

Layer Scan Speed	Hatch Spacing	Overlap	Laser Power	Layer Thickness
1250 mm/s	115 µm	30%	200 W	30 µm

After fabrication, the samples were carefully detached from the substrate via wire electrical discharge machining (wire-EDM). Figure 1 displays images of the Ti6Al4V samples created by the EOS M 280 Metal Print machine at the South-Eastern Applied Materials Research Centre in Ireland and the corresponding CAD model. The surface topology was examined using scanning electron microscopy (SEM). The composition of the powder material used for Ti6Al4V production, based on ASTM F3001-14 standards [31], is listed in Table 1.

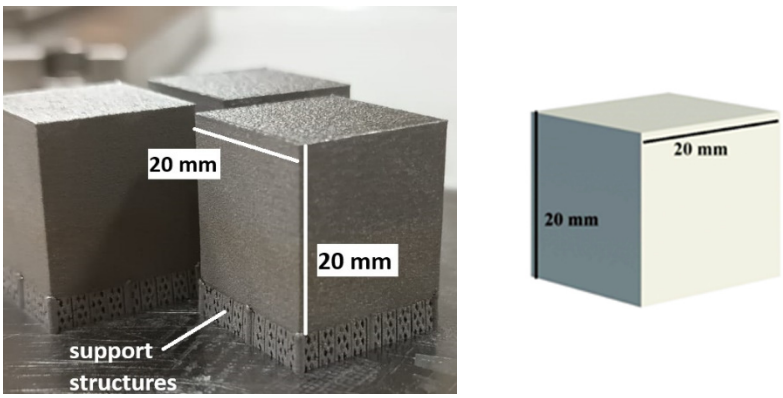

(**a**) (**b**)

Figure 1. (**a**) Samples fabricated via L-PBF; (**b**) AD model created using AutoCAD.

An SBF solution was used as the testing medium in the electrochemical experiments. This solution, prepared by the Element Dudley Lab in the Dudley, UK, was composed according to the specifications and concentrations listed in Table 3. To replicate physiological conditions, the pH of the solution was adjusted to 7.3 using 1 M HCl. All specimens were immersed in this SBF solution and kept at a constant temperature of 37 °C, simulating the human body's environment. Electrochemical tests were conducted under these standardized conditions, as outlined in Table 3. To enable electrical connections for open-circuit potential measurements, a wire was spot-welded onto each sample after a period of six days. Electrochemical tests were carried out in an oxygenated simulated body fluid (SBF) maintained at 37 ± 0.1 °C, which closely resembles human body temperature. Polarization scans were performed according to ASTM G5 Standards [32], with a sweep rate of 0.6 V/h ranging from the corrosion potential (COP) to +1.6 V relative to the standard calomel electrode (SCE). Furthermore, to measure weight loss, the samples were cleaned with deionized water and ethanol after each immersion period to remove any surface contaminants. The initial and final weights of the dried samples were recorded using an analytical balance with a precision of ±0.0001 g. Weight loss was then determined by subtracting the final weight from the initial weight.

Table 3. SBF experimental solutions.

Compound	NaCl	$CaCl_2$	Kill	$NaHCO_3$	$MgCl_2 \cdot 6H_2O$	Na_2SO_4	$K_2HPO_4 \cdot 3H_2O$	Tris
Mass concentration (Moles)	0.137	0.003	0.003	0.004	0.002	0.001	0.001	0.051

3. Results and Discussion

Various surface finishes were applied to as-printed, heat-treated, and reference Ti6Al4V samples to evaluate their influence on corrosion resistance. Confocal microscopy images of the as-printed samples revealed prominent pores and unidirectional scratches on the rough-finished surfaces in L-PBF-fabricated samples. These scratches had depths ranging from approximately 0.3 to 0.5 µm, as indicated by the palette. Samples with a medium surface finish exhibited a smoother texture, though some scratches and surface pores were still present. The differences in manufacturing techniques and resulting microstructural characteristics led to varying levels of corrosion resistance. Figure 2 shows the microscopic voids observed in both types of samples after immersion for the specified durations. It was found that the presence of partially unmelted particles on the surface of L-PBF-manufactured parts is a common defect. These particles are typically not fully melted during the laser scanning due to insufficient energy input or inappropriate scanning parameters. Consequently, they remain loosely attached to the surface or within the material, contributing to surface roughness. Mater et al. [33] stated that the suboptimal surface finish observed in parts produced via L-PBF was primarily due to partially unmelted particles and the balling phenomenon, as depicted in Figure 2. These surface imperfections reduced the available area for cell attachment, resulting in low initial cell adhesion and limited subsequent proliferation. Consequently, this led to the poor biological performance in the as-built samples. Kempen et al. investigated the porosity issue, whether it arises from trapped gas or unmelted powders [34]. Similarly, Martin et al. [35] stated the rough surface finish achieved through L-PBF is due to the presence of partially unmelted particles, as shown in Figure 2. This condition provides inadequate space for cells to attach, leading to poor initial cell adhesion and limited proliferation. Consequently, this results in suboptimal biological behavior in the as-built samples. This illustrates how the surface quality directly impacts cellular responses. A rough surface can hinder the initial attachment of cells, a crucial factor for integrating implants with biological tissues. Additionally, the roughness values recorded were 0.219 µm, 0.282 µm, and 0.371 µm. These values highlight the inherent variability in surface roughness among the samples, which is crucial to the material's performance in corrosive environments.

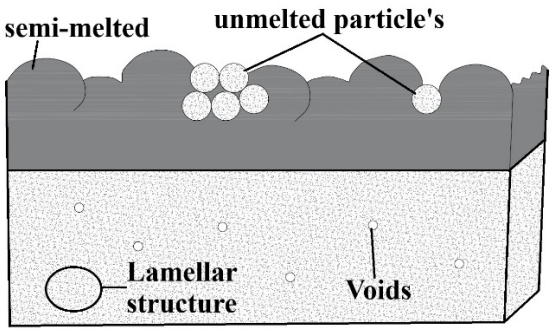

Figure 2. Schematic diagram of surface imperfections of L-PBF-Ti6Al4V.

In orthopedic and dental implants, for instance, surface roughness can impede the process by which bone tissue grows and integrates with the implant. Poor surface finish limits the available surface area for cell attachment and proliferation, which are essential for the stable anchorage of the implant and the promotion of long-term healing. Furthermore, the results discuss the crucial factors for understanding the long-term behavior of Ti6Al4V

in physiological environments. The results reveal significant insights into the degradation mechanisms, which include the formation of voids, exposure of unmelted particles, and the development of pores, all of which have implications for the material's suitability in medical applications. Figure 2 illustrates the typical surface layer configuration after AM, whereas subsequent sections present SEM images showing the surface morphology of a specimen processed with L-PBF.

Furthermore, the schematic highlights the surface defects and irregularities typically observed in AM Ti6Al4V alloys [36]. The cross-sectional view reveals several notable features: semi-melted particles, unmelted powder particles, rough surfaces, lamellar structures, and porosities. These defects contribute to the rough surface, characterized by irregularities and undulations. Fikeni et al. [37] noted that the material exhibits a lamellar structure internally, characteristic of the α+β phase microstructure in Ti6Al4V alloys, which is crucial for understanding the material's mechanical properties. The presence of porosities, represented as small black dots within the lamellar structure, indicates voids or gaps formed during manufacturing. These porosities can significantly impact the alloy's mechanical strength and fatigue resistance [38].

3.1. At the 48 h Mark

After 48 h of exposure, the L-PBF Ti6Al4V samples display a relatively intact surface with some small voids (see Figure 3). The surface appears uniform primarily, indicating that the alloy's inherent corrosion resistance is still largely effective. The small voids observed are indicative of the initial stages of corrosion or could be due to intrinsic defects from the L-PBF process itself.

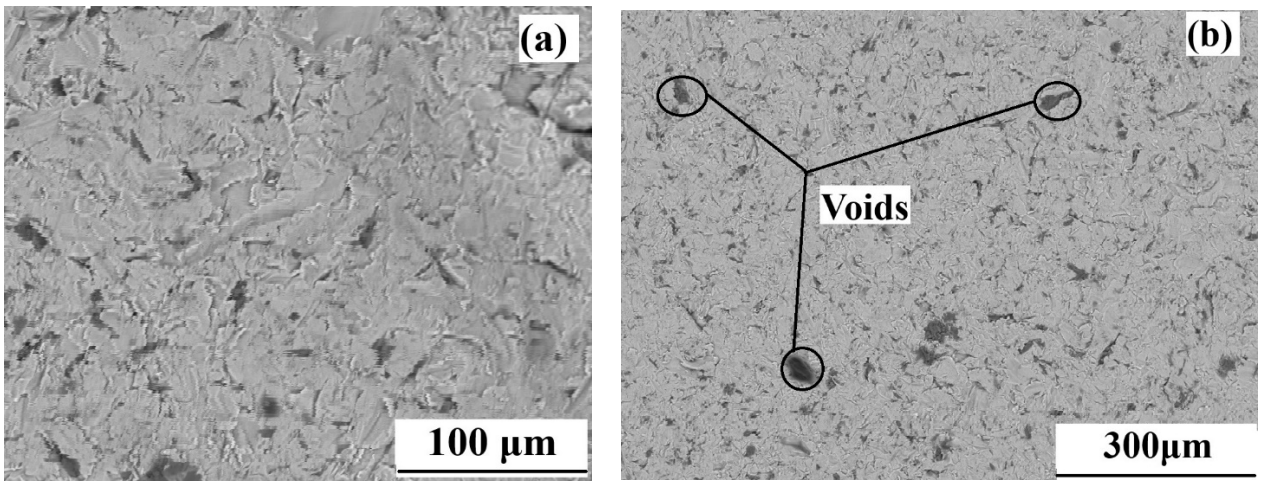

Figure 3. The sample condition after the exposure of 48 h. (**a**) Surface morphology; (**b**) Formation of voids.

These voids suggest minimal penetration of the SBF solution into the material, highlighting that the passive oxide layer, which is primarily composed of titanium dioxide (TiO_2) that forms on the alloy's surface, remains protective. This initial corrosion resistance aligns with findings by Xu et al. [39], who noted that the passive layer in titanium alloys provides substantial protection in chloride-containing environments.

3.2. At the 96 h Mark

Figure 4 shows a noticeable increase in the size and number of voids. Additionally, unmelted particles become more prominent. These particles are remnants of the L-PBF process, where not all powder is completely melted and integrated into the matrix. Their exposure suggests that the passive oxide layer is beginning to fail, allowing the SBF solution to reach and react with these more vulnerable areas. The presence of unmelted particles can be problematic, as they can act as initiation sites for localized corrosion, such as

pitting or crevice corrosion, which are difficult to detect but can severely compromise the material's structural integrity over time. This observation is consistent with research by Hanumantha et al. [40], who identified manufacturing defects, including unmelted particles, as critical factors influencing the corrosion behavior of L-PBF-processed alloys.

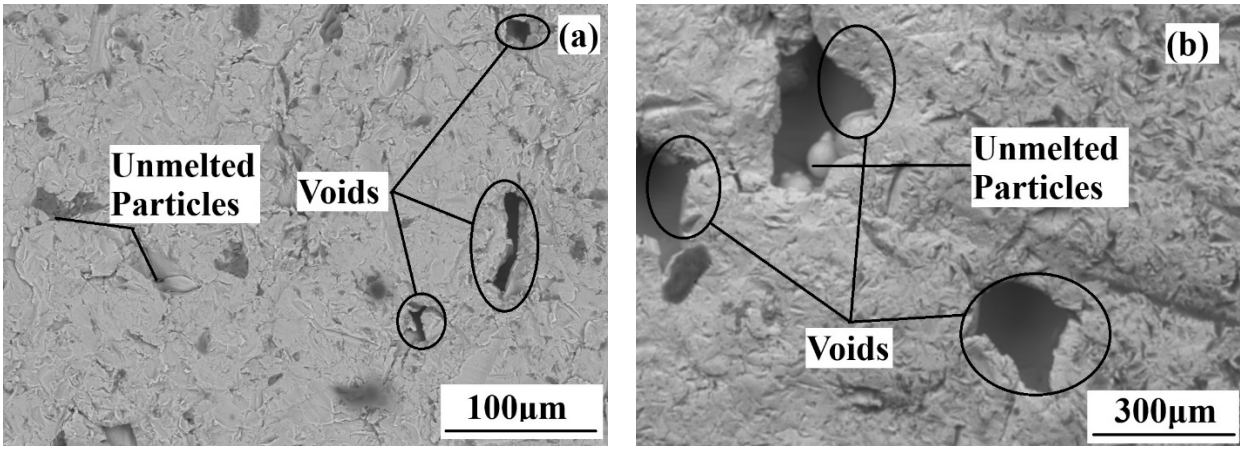

Figure 4. The sample condition after the exposure of 96 h. (**a**) small voids and unmelted particles; (**b**) Larger voids and dispersed unmelted particles.

3.3. At the 144 h Mark

Significant degradation is evident after 144 h of exposure (see Figure 5). The images show a substantial increase in the number and size of voids and the development of pores. In Figure 5, the observed coarse particles are significantly larger than the original powder size, which had an average size between of 26 µm and a maximum of 59 µm. These coarser particles are likely due to spattering during the L-PBF process. Spattering occurs when molten material is ejected from the melt pool due to high energy interactions between the laser and the powder bed. The ejected particles often redeposit on the surface in a solidified state, resulting in particles larger than the original feedstock. This behavior has been noted in previous studies of Ti6Al4V, where spatter particles were found to be larger and chemically similar to the original powder [41,42]. These coarse particles can contribute to surface defects and act as initiation points for localized corrosion, such as pitting, due to their imperfect fusion with the matrix.

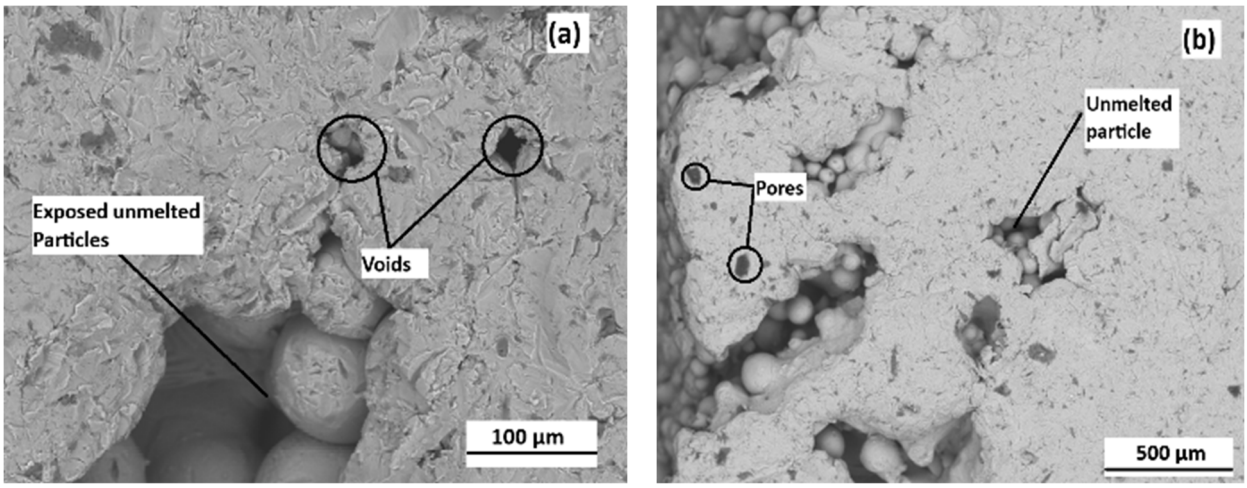

Figure 5. The sample images after the exposure of 144 h. (**a**) Exposed unmelted particles; (**b**) Unmelted particle with visible pores.

Additionally, these larger particles may serve as initiation points for localized corrosion phenomena, such as pitting, due to their inadequate fusion with the surrounding material. These structural changes indicate a severe breakdown of the protective oxide layer, allowing the SBF solution to penetrate the alloy surface extensively. The formation of pores and the increased roughness of the surface suggest aggressive corrosion processes, possibly exacerbated by localized breakdowns of the passive layer. The presence of larger and more exposed unmelted particles also indicates a significant failure of the material's surface integrity. Studies such as those by Bocchetta et al. [43] have shown that prolonged exposure to corrosive environments can lead to the breakdown of passive layers, resulting in accelerated corrosion and structural degradation. The progression of degradation observed in the images corresponds with common corrosion mechanisms in titanium alloys exposed to chloride-containing solutions like SBF. Initially, the passive layer provides good protection; however, over time, localized breakdowns occur, particularly around manufacturing defects such as voids or unmelted particles. These defects can serve as points of weakness where the passive layer is thinner or absent, making them more susceptible to chloride attack, leading to pitting corrosion. Once initiated, pitting can progress rapidly, especially in environments that mimic the human body, which contains chloride ions from bodily fluids. This aligns with findings by Mohsan et al. [44], who emphasized the role of chloride ions in initiating and propagating pitting corrosion in titanium alloys.

3.4. Implications for Biomedical Applications and Manufacturing Considerations

The findings from these observations have important implications for using L-PBF Ti6Al4V in biomedical implants. Although Ti6Al4V initially shows promising corrosion resistance, the rapid degradation observed over longer exposure times raises concerns about its long-term stability in vivo. As Bandyopadhyay et al. [45] indicated, implants must maintain their mechanical integrity and biocompatibility over extended periods, often decades. The increase in voids and the development of pores after 144 h suggest that L-PBF Ti6Al4V may not provide adequate long-term stability without additional surface treatments or coatings. Ralls et al. [46] emphasized that incomplete melting of powder particles can result in structural defects, which can serve as initiation points for corrosion. Ensuring a more homogeneous microstructure with fewer defects enhances the material's performance. Research by Pinto et al. [47] suggests that optimizing L-PBF parameters can significantly reduce defects and improve the mechanical and corrosion properties of Ti6Al4V alloys.

3.5. Corrosion Rate and Weight Loss

At the 48 h mark, the corrosion rate is indicated to be very low, at approximately 0.005 mm/year. Similarly, the weight loss, also an indicator of corrosion activity, is near zero. This minimal change suggests that during the initial 48 h, the Ti6Al4V alloy exhibits good corrosion resistance when exposed to the SBF solution. A passive oxide layer, typically titanium dioxide, likely contributes to this resistance by protecting the underlying material from aggressive ions in the solution [43]. At 96 h, the graph shows a further decrease in the corrosion rate, reaching approximately 0.003 mm/year, and the weight loss remains negligible. This trend indicates that the passive layer on the titanium alloy continues to protect against corrosion, even with prolonged exposure. The slight decrease in corrosion rate might also suggest the continued stabilization of the protective oxide layer, reducing the material's reactivity with the SBF. Figure 6 represents the corrosion rate and weight loss of Ti6Al4V alloy over time when exposed to simulated body fluid.

A significant change is observed after 144 h of exposure. The corrosion rate increases sharply to 0.028 mm/year, and the weight loss also rises dramatically. This sharp increase indicates that the protective oxide layer may have been compromised or that the longer exposure duration has allowed more aggressive ions from the SBF solution to penetrate the layer. Similarly, Hamrahi et al. [48] have discussed the susceptibility of titanium

alloys to localized corrosion once the protective oxide layer is breached, particularly under conditions where chloride ions are present, as these ions can facilitate pitting corrosion.

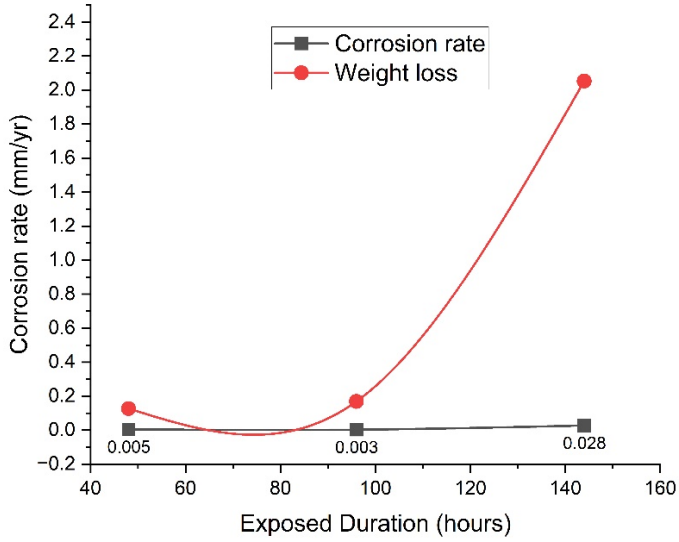

Figure 6. Corrosion rate and weight loss of Ti6Al4V alloy exposed to SBF.

The sudden rise in both corrosion rate and weight loss suggests accelerated material degradation, possibly due to localized corrosion mechanisms such as pitting, which is common in passive metals when the protective layer is damaged. The observed data imply that while the L-PBF Ti6Al4V alloy exhibits good corrosion resistance in the short term, its long-term stability in SBF solution could be a concern, significantly so beyond 100 h of exposure. The initial low corrosion rate and weight loss suggest that the alloy's protective oxide layer effectively prevents corrosion. However, the significant increase in both parameters after extended exposure indicates potential degradation of this protective barrier. This behavior is crucial for biomedical applications, particularly in implants, where long-term material stability is essential. The compromise of the protective oxide layer could increase ion release into the body, potentially causing adverse reactions [49].

3.6. Potentiodynamic Polarization Behavior

Figure 7 illustrates the open-circuit potential (OCP) of Ti6Al4V immersed in simulated body fluid over a 6-day period. The OCP starts at around −260 mV and gradually stabilizes near −190 mV. This trend indicates that the L-PBF Ti6Al4V surface becomes more stable or passivated over time, likely due to the formation of a protective oxide layer. OCP measurements are commonly used to evaluate the corrosion resistance of materials in biological environments, such as orthopedic implants [50].

The increasing OCP suggests enhanced stability, which could improve the material's suitability for use in corrosive environments like the human body [48]. Additionally, initially, the OCP values for L-PBF Ti6Al4V are around −250 mV. The L-PBF Ti6Al4V exhibits a sharp increase in OCP, while other alloys show a more gradual rise. Over the test period, the OCP for L-PBF Ti6Al4V steadily increases, despite minor fluctuations, reaching approximately −190 mV. In contrast, other Ti6Al4V alloys display a more erratic OCP pattern with significant volatility and a notable dip around 400,000 s, indicating a transient electrochemical event, potentially localized corrosion. This dip is followed by a recovery and a final OCP value around −210 mV. The consistent rise in OCP for L-PBF Ti6Al4V suggests the formation of a stable passive oxide layer, indicating superior corrosion resistance.

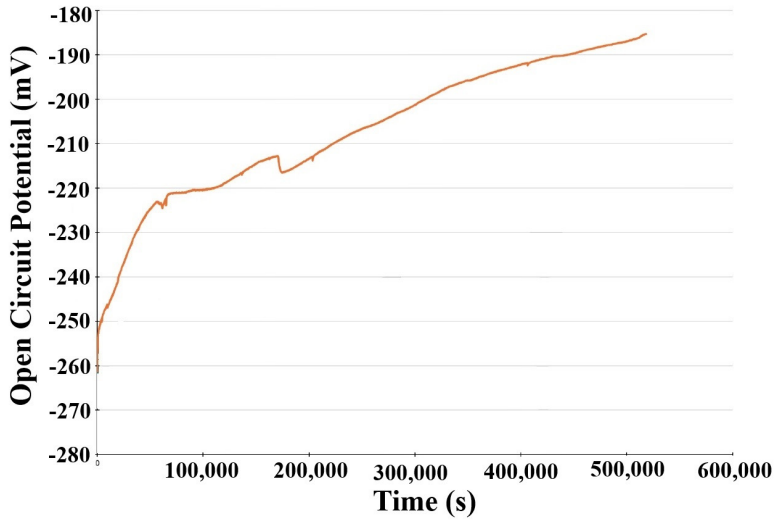

Figure 7. Graph showing the open-circuit potential (OCP) measured over 6 days for L-PBF Ti6Al4V.

In summary, the L-PBF Ti6Al4V alloy shows promising short-term corrosion resistance in SBF, but long-term exposure risks must be addressed. The observed trends underline the importance of thorough material testing under conditions that simulate the intended environment of use to ensure safety and longevity in biomedical applications. In contrast, the presence of partially unmelted particles on the surface can lead to an irregular and non-uniform texture, which offers limited space for cells to attach [51]. This can result in uneven cell distribution and potentially the formation of non-adherent areas, which are detrimental to the overall biological performance of the implant. Moreover, Meng et al. [52] stated that these surface imperfections can act as stress concentrators, where mechanical stresses are localized, potentially leading to early material failure or cracking under load. In the context of biological applications, this not only compromises the structural integrity of the implant but also increases the risk of wear and particle release, which can trigger inflammatory responses or other adverse biological reactions.

4. Conclusions

In conclusion, the widespread use of L-PBF Ti6Al4V in biomedical applications is mainly due to its excellent biocompatibility. However, its vulnerability to localized corrosion, especially pitting, poses a significant challenge. Exposure to chloride ions present in human plasma can damage the alloy's protective oxide layer, leading to corrosion at surface defects and inclusions. These results underscore the necessity of detailed corrosion analysis to ensure the reliability and longevity of biomedical devices made from this alloy. The study also, indicated by the formation of voids, exposure of unmelted particles, and pore development, highlights the challenges in using this alloy for biomedical purposes.

(1) The study observed a weight loss of 0.0049 g and a corrosion rate of 0.028 mm/year, highlighting the importance of thoroughly testing L-PBF Ti6Al4V in SBF.
(2) The presence voids, unmelted particles, and pores were identified as key factors contributing to localized corrosion and pose challenges to the material's structural integrity and longevity in biomedical applications.
(3) The research demonstrated that while L-PBF Ti6Al4V initially exhibits good corrosion resistance, it deteriorates significantly over time.
(4) The study's outcomes are particularly relevant for designing implants, where ensuring long-term stability and reliability is crucial. Insights into the degradation mechanisms of L-PBF Ti6Al4V in environments mimicking body conditions are essential for developing more durable implants.

(5) The findings suggest that optimizing L-PBF process parameters can significantly reduce microstructural defects, enhancing the corrosion resistance and overall performance of Ti6Al4V implants.

5. Future Research Directions

Future studies should aim to develop advanced surface treatments and coatings to provide better corrosion protection for L-PBF Ti6Al4V alloys. Additionally, exploring the effects of various L-PBF parameters on microstructural properties and corrosion behavior is crucial. Research into the long-term biological impacts of corrosion by-products on tissue integration and patient safety will also be critical to advancing these materials' safe and effective use in biomedical applications.

Author Contributions: In the collaborative development of this journal article, each contributor played a crucial role in its conception, drafting, and refinement. The authors' combined expertise and commitment to the subject matter formed the basis of this work. S.P. took the lead in writing the article, while X.V. and W.S. made significant contributions through their active involvement in the review process. Their constructive feedback and assessments significantly improved the quality of the manuscript. All authors have read and agreed to the published version of the manuscript.

Funding: This research received no external funding.

Data Availability Statement: All relevant data are included within the manuscript. No additional data are available.

Conflicts of Interest: The authors declare no conflicts of interest.

References

1. Marin, E.; Lanzutti, A. Biomedical Applications of Titanium Alloys: A Comprehensive Review. *Materials* **2023**, *17*, 114. [CrossRef] [PubMed]
2. Soundararajan, S.R.; Vishnu, J.; Manivasagam, G.; Muktinutalapati, N.R. Processing of beta titanium alloys for aerospace and biomedical applications. In *Titanium Alloys-Novel Aspects of Their Manufacturing and Processing*; IntechOpen: London, UK, 2018.
3. Moghadasi, K.; Isa, M.S.M.; Ariffin, M.A.; Jamil, M.Z.M.; Raja, S.; Wu, B.; Yamani, M.; Bin Muhamad, M.R.; Yusof, F.; Jamaludin, M.F.; et al. A review on biomedical implant materials and the effect of friction stir based techniques on their mechanical and tribological properties. *J. Mater. Res. Technol.* **2022**, *17*, 1054–1121. [CrossRef]
4. Geetha, M.; Singh, A.K.; Asokamani, R.; Gogia, A.K. Ti based biomaterials, the ultimate choice for orthopaedic implants–a review. *Prog. Mater. Sci.* **2009**, *54*, 397–425. [CrossRef]
5. Abdudeen, A.; Abu Qudeiri, J.E.; Kareem, A.; Valappil, A.K. Latest developments and insights of orthopedic implants in biomaterials using additive manufacturing technologies. *J. Manuf. Mater. Process.* **2022**, *6*, 162. [CrossRef]
6. Aufa, A.; Hassan, M.Z.; Ismail, Z. Recent advances in Ti-6Al-4V additively manufactured by selective laser melting for biomedical implants: Prospect development. *J. Alloys Compd.* **2022**, *896*, 163072. [CrossRef]
7. Shidid, D.P. Design and Manufacture of Patient Specific Orthopaedic Implants Using Selective Laser Melting (SLM) Technology. Doctoral Dissertation, RMIT University, Melbourne, Australia, 2016.
8. Mahale, R.S.; Shamanth, V.; Hemanth, K.; Nithin, S.; Sharath, P.; Shashanka, R.; Patil, A.; Shetty, D. Processes and applications of metal additive manufacturing. *Mater. Today Proc.* **2022**, *54*, 228–233. [CrossRef]
9. Mahamood, R.M.; Akinlabi, E.T.; Shukla, M.; Pityana, S. Revolutionary Additive Manufacturing: An Overview. *Lasers Eng. (Old City Publ.)* **2014**, *27*, 161.
10. Jayawardane, H.; Davies, I.J.; Gamage, J.; John, M.; Biswas, W.K. Sustainability perspectives—A review of additive and subtractive manufacturing. *Sustain. Manuf. Serv. Econ.* **2023**, *2*, 100015. [CrossRef]
11. Nguyen, H.D.; Pramanik, A.; Basak, A.; Dong, Y.; Prakash, C.; Debnath, S.; Shankar, S.; Jawahir, I.; Dixit, S.; Buddhi, D. A critical review on additive manufacturing of Ti-6Al-4V alloy: Microstructure and mechanical properties. *J. Mater. Res. Technol.* **2022**, *18*, 4641–4661. [CrossRef]
12. Vaz, R.F.; Garfias, A.; Albaladejo, V.; Sanchez, J.; Cano, I.G. A Review of Advances in Cold Spray Additive Manufacturing. *Coatings* **2023**, *13*, 267. [CrossRef]
13. Fischer, D.; Cheng, K.-Y.; Neto, M.Q.; Hall, D.; Bijukumar, D.; Orías, A.A.E.; Pourzal, R.; van Arkel, R.J.; Mathew, M.T. Corrosion Behavior of Selective Laser Melting (SLM) Manufactured Ti6Al4V Alloy in Saline and BCS Solution. *J. Bio-Tribo-Corros.* **2022**, *8*, 63. [CrossRef] [PubMed]
14. Hamza, H.M.; Deen, K.M.; Khaliq, A.; Asselin, E.; Haider, W. Microstructural, corrosion and mechanical properties of additively manufactured alloys: A review. *Crit. Rev. Solid State Mater. Sci.* **2022**, *47*, 46–98. [CrossRef]

15. Qian, C.; Xu, H.; Zhong, Q. The influence of process parameters on corrosion behavior of Ti6Al4V alloy processed by selective laser melting. *J. Laser Appl.* **2020**, *32*, 032010. [CrossRef]
16. Sola, A.; Nouri, A. Microstructural porosity in additive manufacturing: The formation and detection of pores in metal parts fabricated by powder bed fusion. *J. Adv. Manuf. Process.* **2019**, *1*, 10021. [CrossRef]
17. Huang, S.; Wu, W.; Su, Y.; Qiao, L.; Yan, Y. Insight into the corrosion behaviour and degradation mechanism of pure zinc in simulated body fluid. *Corros. Sci.* **2021**, *178*, 109071. [CrossRef]
18. Yang, J.; Song, Y.; Dong, K.; Han, E.-H. Research progress on the corrosion behavior of titanium alloys. *Corros. Rev.* **2023**, *41*, 5–20. [CrossRef]
19. Atapour, M.; Pilchak, A.; Frankel, G.; Williams, J. Corrosion behavior of β titanium alloys for biomedical applications. *Mater. Sci. Eng. C* **2011**, *31*, 885–891. [CrossRef]
20. Das, P.; Kumar, T.S.S.; Sahu, K.K.; Gollapudi, S. Corrosion, stress corrosion cracking and corrosion fatigue behavior of magnesium alloy bioimplants. *Corros. Rev.* **2022**, *40*, 289–333. [CrossRef]
21. Oliveira, N.; Guastaldi, A. Electrochemical stability and corrosion resistance of Ti–Mo alloys for biomedical applications. *Acta Biomater.* **2009**, *5*, 399–405. [CrossRef]
22. Zhao, C.; Bai, Y.; Zhang, Y.; Wang, X.; Xue, J.M.; Wang, H. Influence of scanning strategy and building direction on microstructure and corrosion behaviour of selective laser melted 316L stainless steel. *Mater. Des.* **2021**, *209*, 109999. [CrossRef]
23. Attar, H.; Ehtemam-Haghighi, S.; Kent, D.; Okulov, I.V.; Wendrock, H.; Bönisch, M.; Volegov, A.S.; Calin, M.; Eckert, J.; Dargusch, M.S. Nanoindentation and wear properties of Ti and Ti-TiB composite materials produced by selective laser melting. *Mater. Sci. Eng. A* **2017**, *688*, 20–26. [CrossRef]
24. Malekipour, E.; El-Mounayri, H. Common defects and contributing parameters in powder bed fusion AM process and their classification for online monitoring and control: A review. *Int. J. Adv. Manuf. Technol.* **2018**, *95*, 527–550. [CrossRef]
25. Chandramohan, P.; Bhero, S.; Obadele, B.A.; Olubambi, P.A. Laser additive manufactured Ti–6Al–4V alloy: Tribology and corrosion studies. *Int. J. Adv. Manuf. Technol.* **2017**, *92*, 3051–3061. [CrossRef]
26. Bai, Y.; Gai, X.; Li, S.; Zhang, L.-C.; Liu, Y.; Hao, Y.; Zhang, X.; Yang, R.; Gao, Y. Improved corrosion behaviour of electron beam melted Ti-6Al–4V alloy in phosphate buffered saline. *Corros. Sci.* **2017**, *123*, 289–296. [CrossRef]
27. *ASTM E29 Standards*; Standard Practice for Using Significant Digits in Test Data to Determine Conformance with Specifications. ASTM International: West Conshohocken, PA, USA, 2013.
28. *ASTM B212-21*; Standard Test Method for Apparent Density of Free-Flowing Metal Powders Using the Hall Flowmeter Funnel. ASTM International: West Conshohocken, PA, USA, 1999; Volume 2, pp. 89–91. [CrossRef]
29. Enterprise Ireland Technology Gateway Network. Available online: https://seam.ie/ (accessed on 23 September 2024).
30. Lu, P.; Wu, M.; Liu, X.; Duan, W.; Han, J. Study on corrosion resistance and bio-tribological behavior of porous structure based on the SLM manufactured medical Ti6Al4V. *Met. Mater. Int.* **2020**, *26*, 1182–1191. [CrossRef]
31. *ASTM F3001-14*; Standard Specification for Additive Manufacturing Titanium-6 Aluminum-4 Vanadium ELI (Extra Low Interstitial) with Powder Bed Fusion. ASTM International: West Conshohocken, PA, USA, 2014.
32. *ASTM G5-13e1*; Standard Reference Test Method for Making Potentiodynamic Anodic Polarization Measurements: Designation. ASTM International: West Conshohocken, PA, USA, 2013. [CrossRef]
33. Jamshidi, P.; Aristizabal, M.; Kong, W.; Villapun, V.; Cox, S.C.; Grover, L.M.; Attallah, M.M. Selective laser melting of Ti6Al4V: The impact of post-processing on the tensile, fatigue and biological properties for medical implant applications. *Materials* **2020**, *13*, 2813. [CrossRef]
34. Kempen, K.; Thijs, L.; Van Humbeeck, J.; Kruth, J.-P. Processing AlSi10Mg by selective laser melting: Parameter optimisation and material characterisation. *Mater. Sci. Technol.* **2015**, *31*, 917–923. [CrossRef]
35. Martin, J.Y.; Schwartz, Z.; Hummert, T.W.; Schraub, D.M.; Simpson, J.; Lankford Jr, J.; Dean, D.D.; Cochran, D.L.; Boyan, B. Effect of titanium surface roughness on proliferation, differentiation, and protein synthesis of human osteoblast-like cells (MG63). *J. Biomed. Mater. Res.* **1995**, *29*, 389–401. [CrossRef]
36. Okuniewski, W.; Walczak, M.; Szala, M. Effects of Shot Peening and Electropolishing Treatment on the Properties of Additively and Conventionally Manufactured Ti6Al4V Alloy: A Review. *Materials* **2024**, *17*, 934. [CrossRef]
37. Fikeni, L. Microstructural Evolution and Its Influence on Mechanical Properties of Ti-Nb Binary Alloys. Master's Thesis, University of Pretoria, Pretoria, South Africa, 2021.
38. Li, F.; Li, J.; Kou, H.; Zhou, L. Porous Ti6Al4V alloys with enhanced normalized fatigue strength for biomedical applications. *Mater. Sci. Eng. C* **2016**, *60*, 485–488. [CrossRef]
39. Xu, K.; Lan, A.; Qiao, J.; Yang, H.; Han, P.; Liaw, P. Corrosion behaviors and mechanisms of in-situ Ti-based MGMCs in chloride-containing and chloride-free solutions. *Intermetallics* **2019**, *105*, 179–186. [CrossRef]
40. Hanumantha, M. Investigation of the Microstructural and Mechanical Properties of Selectively Laser Melted IN718 Overhangs Fabricated without Support Structures. Master's Thesis, The University of Texas at Arlington, Arlington, TX, USA, 2021.
41. Keaveney, S.; Shmeliov, A.; Nicolosi, V.; Dowling, D.P. Investigation of process by-products during the Selective Laser Melting of Ti6AL4V powder. *Addit. Manuf.* **2020**, *36*, 101514. [CrossRef]
42. Rothfelder, R.; Huber, F.; Schmidt, M. Influence of beam shape on spatter formation during PBF-LB/M of Ti6Al4V and tungsten powder. *Procedia CIRP* **2022**, *111*, 14–17. [CrossRef]

43. Bocchetta, P.; Chen, L.-Y.; Tardelli, J.D.C.; dos Reis, A.C.; Almeraya-Calderón, F.; Leo, P. Passive layers and corrosion resistance of biomedical Ti-6Al-4V and β-Ti alloys. *Coatings* **2021**, *11*, 487. [CrossRef]
44. Mohsan, A.U.H.; Wei, D. Advancements in Additive Manufacturing of Tantalum via the Laser Powder Bed Fusion (PBF-LB/M): A Comprehensive Review. *Materials* **2023**, *16*, 6419. [CrossRef]
45. Bandyopadhyay, A.; Mitra, I.; Goodman, S.B.; Kumar, M.; Bose, S. Improving biocompatibility for next generation of metallic implants. *Prog. Mater. Sci.* **2023**, *133*, 101053. [CrossRef] [PubMed]
46. Ralls, A.M.; John, M.; Noud, J.; Lopez, J.; LeSourd, K.; Napier, I.; Hallas, N.; Menezes, P.L. Tribological, Corrosion, and Mechanical Properties of Selective Laser Melted Steel. *Metals* **2022**, *12*, 1732. [CrossRef]
47. Pinto, T.; CG, R.; MJ, R. Comparative study on manufacturing of EDM electrodes by laser sintering process. *Eng. Res. Express* **2024**, *6*, 035501. [CrossRef]
48. Hamrahi, B.; Yarmand, B.; Massoudi, A. Improved in-vitro corrosion performance of titanium using a duplex system of plasma electrolytic oxidation and graphene oxide incorporated silane coatings. *Surf. Coat. Technol.* **2021**, *422*, 127558. [CrossRef]
49. Pal, S.; Velay, X.; Saleem, W. Investigation into the Electrochemical Corrosion Characteristics of As-Built SLM Ti-6Al-4 V Alloy in Electrolytic Environments. *J. Bio-Tribo-Corros.* **2024**, *10*, 1–11. [CrossRef]
50. Souza, J.C.M.; Apaza-Bedoya, K.; Benfatti, C.A.M.; Silva, F.S.; Henriques, B. A Comprehensive Review on the Corrosion Pathways of Titanium Dental Implants and Their Biological Adverse Effects. *Metals* **2020**, *10*, 1272. [CrossRef]
51. Jøraholmen, T. Differentiation and Bone Deposition of Bone Marrow Derived Stem Cells on Additive Manufactured Porous Ti6Al4V Scaffolds. Master's Thesis, NTNU, Trondheim, Norway, 2017.
52. Meng, L.; Yang, H.; Ben, D.; Ji, H.; Lian, D.; Ren, D.; Li, Y.; Bai, T.; Cai, Y.; Chen, J.; et al. Effects of defects and microstructures on tensile properties of selective laser melted Ti6Al4V alloys fabricated in the optimal process zone. *Mater. Sci. Eng. A* **2021**, *830*, 142294. [CrossRef]